Single-Molecule Interfacial Electron Transfer Dynamics of Porphyrin on TiO2 Nanoparticles: Dissecting the Complex Electronic Coupling Dependent Dynamics

ARTICLE *in* THE JOURNAL OF PHYSICAL CHEMISTRY C · AUGUST 2014

Impact Factor: 4.77 · DOI: 10.1021/jp506199w

4 AUTHORS:

Vishal Govind Rao
Bowling Green State University
49 PUBLICATIONS **530** CITATIONS
SEE PROFILE

Bharat Dhital
Bowling Green State University
4 PUBLICATIONS **5** CITATIONS
SEE PROFILE

Yufan He
Bowling Green State University
38 PUBLICATIONS **680** CITATIONS
SEE PROFILE

H Peter Lu
Bowling Green State University
118 PUBLICATIONS **3,961** CITATIONS
SEE PROFILE

THE JOURNAL OF PHYSICAL CHEMISTRY C

Article

pubs.acs.org/JPCC

Single-Molecule Interfacial Electron Transfer Dynamics of Porphyrin on TiO_2 Nanoparticles: Dissecting the Complex Electronic Coupling Dependent Dynamics

Vishal Govind Rao, Bharat Dhital, Yufan He, and H. Peter Lu*

Department of Chemistry and Center for Photochemical Sciences, Bowling Green State University, Bowling Green, Ohio 43403, United States

Supporting Information

ABSTRACT: The photosensitized interfacial electron transfer (ET) dynamics of the zinc(II)−5,10,15,20-tetra(3-carboxyphenyl)porphyrin (*m*-ZnTCPP)−TiO_2 nanoparticle (NP) system has been studied using single-molecule photon-stamping spectroscopy. The single-molecule fluorescence intensity trajectories of *m*-ZnTCPP on TiO_2 NP surface show fluctuations and blinking between bright and dark states, which are attributed to the variations in the reactivity of interfacial ET, i.e., intermittent interfacial electron transfer dynamics. Comparing the results with that from our earlier studied *p*-ZnTCPP−TiO_2 nanoparticle system, we show the effect of anchoring group binding geometry (meta or para), hence electronic coupling of sensitizer (*m*-/*p*-ZnTCPP) and TiO_2 substrate, on interfacial ET dynamics. Compared to *p*-ZnTCPP on TiO_2 NP surface, with *m*-ZnTCPP, dark states are observed to dominate in single-molecule fluorescence intensity trajectories. This observation coupled with the large difference in lifetime derived from bright and dark states of *m*-ZnTCPP demonstrates higher charge injection efficiency of *m*-ZnTCPP than *p*-ZnTCPP. The nonexponential autocorrelation function decay and the power-law distribution of the dark-time probability density provide a detailed characterization of the inhomogeneous interfacial ET dynamics. The distribution of autocorrelation function decay times (τ) and power-law exponents (m_{dark}) for *m*-ZnTCPP are found to be different from those for *p*-ZnTCPP, which indicates the sensitivity of τ and m_{dark} on the molecular structure, molecular environment, and molecule−substrate electronic coupling of the interfacial electron transfer dynamics. Overall, our results strongly suggest that the fluctuation and even intermittency of excited-state chemical reactivity are intrinsic and general properties of molecular systems that involve strong molecule−substrate interactions.

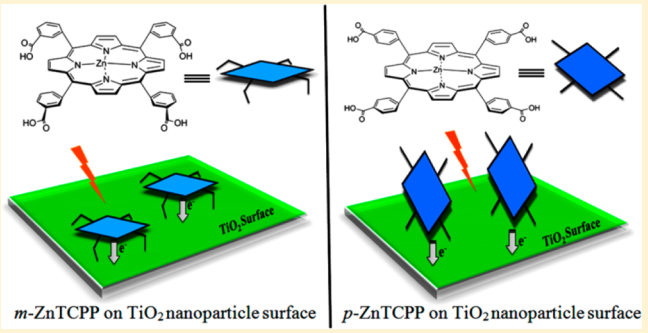

1. INTRODUCTION

Interfacial electron transfer plays a critical role in surface chemistry, catalysis, and solar energy conversion, including solar photovoltaic and solar fuel science and technology.[1−18] However, typical interfacial electron transfer (ET) dynamics in such chemical systems often involve temporal fluctuations and nanoscale spatial heterogeneities, i.e., the dynamic disorder and static disorder,[7,9,19] presenting a high challenge for ensemble-averaged experiments for a molecular level characterization. To optimize the factors that influence interfacial electron transfer dynamics, it is essential to first experimentally measure the effects of the key physical parameters on the interfacial electron transfer dynamics. The parameters which greatly influence ET dynamics include electronic coupling between the molecule and semiconductor, vibrational relaxation energy of adsorbed molecule, solvent reorganization energy, driving force of the free energy gap, the surface structures, and the defect surface states.[19−22] Presumably, the understanding should come both from spatially larger scales for distributions and domain and from molecular scales for molecular structures of both the molecules and the substrate surfaces. Dye-sensitized solar cell (DSSC) systems containing a semiconductor with wide band gap, such as TiO_2,[9,23−36] SnO_2,[37−39] ZrO_2,[40−43] and ZnO,[40,44,45] have wider applications in solar energy conversion systems in the development of the solar photovoltaic, solar fuel, and photocatalytic environmental sciences and technology.[1−6,9,13,46−51]

In general, a typical DSSC system consists of a dye molecule anchored to the semiconductor TiO_2 nanoparticle surface through an anchoring group of the dye. Upon excitation, an electron populates the lowest unoccupied molecular orbital (LUMO) and initiates the forward electron transfer (FET) from the molecular excited states to the conduction band or energetically accessible surface states of semiconductor nanoparticles (NPs). Following FET, the injected electrons go through different semiconductor processes such as charge trapping, detrapping, and electron Brownian and non-Brownian diffusion before (i) recombination with parent cation (back-

Received: June 22, 2014
Revised: August 5, 2014
Published: August 8, 2014

   dx.doi.org/10.1021/jp506199w | J. Phys. Chem. C 2014, 118, 20209−20221

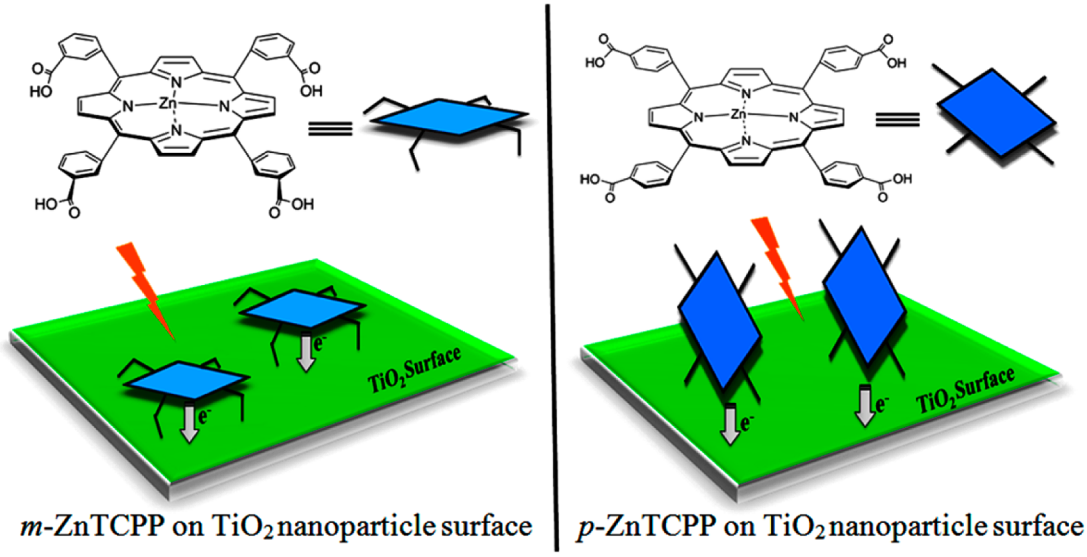

Figure 1. Schematic representation of *m*-ZnTCPP and *p*-ZnTCPP binding on the TiO_2 surface. The different molecular binding geometries on the TiO_2 surface contribute to different electronic couplings between the molecules and the substrate, and in turn, contribute to different interfacial electron transfer rate processes.

ET,BET) or (ii) diffusion away to generate photovoltaic potential energy.[19−21,52,53] Unlike FET dynamics, which are predominately ultrafast in the femtosecond to several hundred picoseconds range,[9,33,36,42,43] BET dynamics is often non-exponential[12,33,54−59] or stretched exponential[60−64] ranging from sub-nanoseconds to several milliseconds.[9,36,42] In an efficient DSSC, proper control of both FET and BET is desirable.

The interfacial ET dynamics were found to be inhomogeneous from molecule to molecule and at various time points, showing significant static and dynamic disorder that is difficult to analyze by conventional ensemble-averaged measurements.[57,65−70] Generally, ensemble-averaged measurements often encounter interferences from molecular aggregation, multiple electron injection to a single particle, and multiple electron cation recombinations on the surface of a single particle. Single-molecule spectroscopy,[9,66,71−82] coupled with scanning confocal fluorescence microscopy and photon-stamping technique is capable of studying one molecule at a time in a specific nanoscale local environment.

The electronic coupling strength between excited states of dye molecule and the semiconductor can be modified through a number of ways including (i) the use of a bridge between the chromophore and the anchoring group of the dye molecule; (ii) the use of different anchoring groups, such as carboxylic acid, hydroxyl, sulfonic acid, phosphonic acid, salicylate, and acetylacetonate derivatives; and (iii) the use of different numbers of anchoring groups such as bipodal, tripodal, and tetrapodal.[19,36,83] Carboxylic acid and phosphonic acid functionalities have been shown to be the most effective anchoring groups, from which the carboxylic acid anchor has emerged as the most popular and widely used choice.[19,36,83] The mode of attachment and the position of these anchoring groups also affect the coupling strength between the excited states of the dye molecule and the semiconductor.[19] In this work we have probed the effect of anchoring group position on interfacial ET dynamics. The interfacial ET between different derivatives of Zn-porphyrin on TiO_2 has been extensively studied at the ensemble-averaged level.[40,83−87] For example, using different derivatives of Zn-porphyrin as a sensitizer, an efficiency as high as 12−13% was reported.[46,47] These studies demonstrated the Zn-Porphyrin−TiO_2 system as an efficient photosensitization solar energy conversion system.[83−86] It has been also shown that the position of the carboxylic acid anchoring groups on the *meso*-phenyl rings of the porphyrin macrocycle plays an important role on the binding mode and as a result on the electronic coupling of dye−TiO_2 and other fundamental properties regulating the interfacial electron transfer dynamics.[40,86] In our previous report, the interfacial ET dynamics of the zinc(II)−5,10,15,20-tetra(4-carboxyphenyl)porphyrin (*p*-ZnTCPP)−TiO_2 NP system was studied at the single-molecule level.[79] On the basis of our earlier reports,[79,80] we concluded that the highly inhomogeneous ET dynamics are commonly observed in interfacial chemical reactions, strongly regulated by the molecular interaction between adsorbed molecule and substrate surface. Rochford et al.[40] studied the photoelectrochemical properties of *m*-ZnTCPP and *p*-ZnTCPP on different metal oxides surfaces. Their studies suggest that the four anchoring groups (-COOH group) in the meta-position of *meso*-phenyl rings of the porphyrin macrocycle get directly attached to the metal oxide surface and facilitate a planar binding geometry (Figure 1).[40,86] The computer modeling, which also studies these molecules on a single-molecular level, predicts planar vs standing conformation of the *m*-ZnTCPP vs *p*-ZnTCPP.[40,88] Carrying out different ensemble-averaged experiments, Rochford et al.[40] also demonstrated higher photocurrent conversion efficiency of *m*-ZnTCPP compared to *p*-ZnTCPP. Although bulk properties provide useful information about the system of interest, the static disorder and dynamic disorder can be better characterized by single-molecule spectroscopy experiments as powerful and complementary approaches.[74−77,79,80] Here, we report our studies of single-molecule interfacial electron transfer dynamics and mechanism of the zinc(II)−5,10,15,20-tetra(3-carboxyphenyl) porphyrin (*m*-ZnTCPP)−TiO_2 NP system by specifically probing the effect of the anchoring group position (meta or para), hence molecular interaction

dx.doi.org/10.1021/jp506199w | J. Phys. Chem. C 2014, 118, 20209−20221

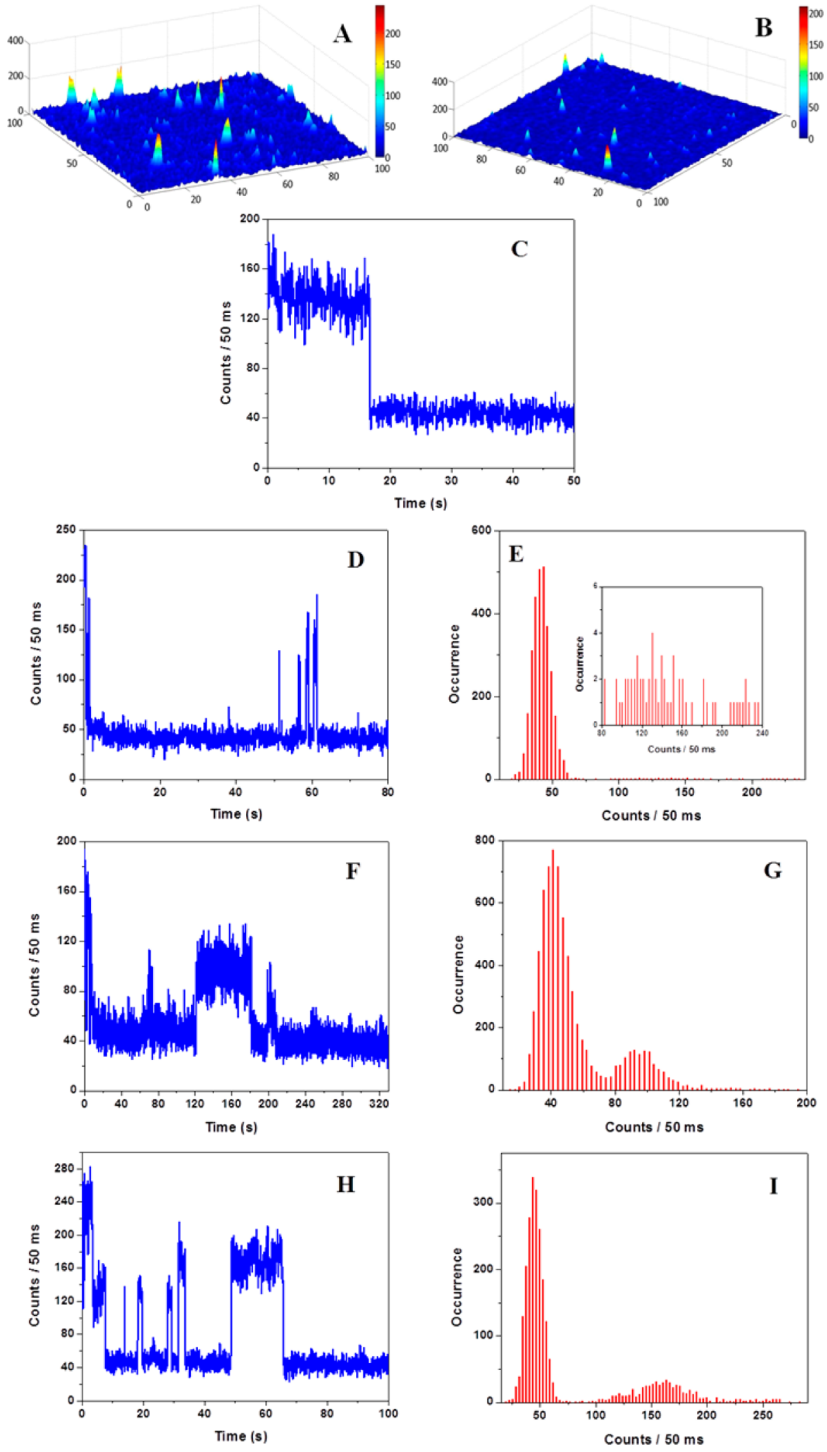

Figure 2. Confocal fluorescence images of *m*-ZnTCPP on (A) bare cover glass and (B) TiO_2 NPs-coated cover glass (image sizes, 20 μm × 20 μm and 100 × 100 pixels). Fluorescence emission trajectories of *m*-ZnTCPP on (C) bare cover glass and (D, F, H) TiO_2 NPs-coated cover glass. Histograms of the emission intensity (E, G, I) are shown to determine the threshold for bright and dark states.

between dye and TiO_2 nanoparticle on the inhomogeneous interfacial ET reactivity.

2. EXPERIMENTAL SECTION

2.1. Materials and Sample Preparation. *m*-ZnTCPP and dichloromethane were purchased from Frontier Scientific (research and development purpose only) and EMD chemicals (HPLC grade), respectively. Ethanol (200 proof; anhydrous, ≥99.5%) and poly(methyl methacrylate) (PMMA; MW 15000 g mol^{-1}) were purchased from Aldrich. All of the reagents were used as received. Cover glasses (Fisher) were thoroughly cleaned by sonication in deionized water, ethanol, acetone (CHROMASOLV Plus, for HPLC; ≥99.5%; Aldrich), and deionized water, respectively, each for 20 min, and then dried using a nitrogen gas before their use. Nanometer-size TiO_2 particles were prepared by the hydrolysis of titanium isopropoxide (Aldrich, 99.999%) as precursor according to a literature protocol.[89] The size range (diameter) of the TiO_2

dx.doi.org/10.1021/jp506199w | J. Phys. Chem. C 2014, 118, 20209−20221

nanoparticles was found to be 10−15 nm, as determined by atomic force microscopy (AFM) and scanning electron microscopy (SEM). For the single-molecule experiments, we prepared the sample following our earlier reported procedures.[79,80] Briefly, for a control experiment, 25 μL of 0.1 nM *m*-ZnTCPP in ethanol solution was first spin-coated on a clean cover glass (Fisher; 18 mm × 18 mm; thickness, 170 μm) at 3000 rpm and covered by spin coating 50 μL PMMA (in CH_2Cl_2, 1 mg/mL) to form a thin film to protect the dye molecules from singlet O_2 photobleaching. The sample of *m*-ZnTCPP on TiO_2 NPs for interfacial ET study was prepared by first spin coating 25 μL of TiO_2 NP solution on a clean cover glass (Fisher; 18 mm × 18 mm; thickness, 170 μm) at 3000 rpm followed by overlaying 25 μL of 0.1 nM *m*-ZnTCPP in ethanol and 50 μL of PMMA (in CH_2Cl_2, 1 mg/mL) by spin coating at 3000 rpm. To consider the purity of the reagents used and their effect on spectroscopic measurements, we have shown a confocal image from a control experiment (Figure S1 of Supporting Information), where a blank ethanol solution is spin-coated on a clean cover glass followed by spin coating 50 μL of PMMA (in CH_2Cl_2, 1 mg/mL) to form a thin film.

2.2. Single-Molecule Fluorescence Spectroscopy and Imaging. We studied the single-molecule interfacial ET dynamics of *m*-ZnTCPP−TiO_2 NP system using single-molecule photon-stamping spectroscopic approach capable of recording each detected photon with its chronic arrival time (absolute arrival time) and the time delay between the photoexcitation and emission of the specific exited state of the individual molecule.[79,80,90] A 76 MHz femtosecond Ti:sapphire laser (Coherent Mira 900 D; 1.6 W; 200 fs full width at half-maximum (fwhm)) was used to pump an optical parametric oscillator (APE-OPO, Coherent Inc.), and the output signal from the OPO was frequency-doubled to 532 nm using a lithium triborate (LBO) nonlinear optical crystal, which was used as the excitation source. To eliminate the fundamental IR light, the beam passed through a pair of prisms and was then delivered in to an Axiovert 135 inverted scanning confocal microscope equipped with a 100 × 1.3 numerical aperture (NA) oil immersion objective (Zeiss FLUAR) and a close-loop nanoscale-precision piezoelectric scanning stage (PI (Physik Instrumente) L.P.) to control the position of a sample. A beam splitter Z532rdc (Chroma) was used to reflect the excitation light into the objective (excitation spot size ∼ 300 nm; excitation power at the sample was kept between 200 and 300 nW). The emission light passed through the emission filter HQ545lp (Chroma, for *m*-ZnTCPP, and the emission wavelength typically ranges from 570 to 750 nm: the absorption and emission spectra of *m*-ZnTCPP and *m*-ZnTCPP bound to TiO_2 in ethanol are shown in Figure S2 of Supporting Information) and collected by a single-photon counting avalanche photodiode (APD) detector (PerkinElmer SPCMAQR-14; pinhole size of APD is 170 μm). Photon-stamping data were recorded by a time-correlated single-photon counting (TCSPC) system (SPC-830, Becker & Hickl GmbH) in a FIFO (first-in first-out) mode.

3. RESULTS AND DISCUSSION

The interfacial ET across dye molecule−semiconductor interface represents one of the most important chemical processes in surface redox chemistry, photocatalysis, and solar energy conversion. Sufficient understanding of interfacial ET reactivity and factors influencing the ET reactivity is crucial to fundamental sciences as well as to solar cell and solar fuel technology developments. Earlier, we reported our work on systematic investigation and analysis of single-molecule interfacial electron transfer dynamics regulated by vibrational relaxation energy, vibronic coupling, and Franck−Condon factors.[79,80,90−93] We have revealed the high inhomogeneity of the vibrational relaxation energy and characterized the inhomogeneity's impact on the measured static and dynamic disordered single-molecule interfacial electron transfer dynamics. Identifying the intermittency[94−97] of the single-molecule interfacial electron transfer dynamics, we advanced a critical understanding of the complex nonexponential interfacial electron transfer dynamics reported widely over the years by time-resolved ensemble-averaged experiments from nanosecond to femtosecond time scales.[79,80,91−93] Here we advance the understanding of interfacial ET reactivity by showing the effect of molecule−TiO_2 surface interactions on interfacial ET dynamics using single-molecule spectroscopy, aiming to shed light on the electronic coupling dependence of the interfacial electron transfer dynamics. Parts A and B of Figure 2 show the single-molecule fluorescence images of *m*-ZnTCPP on bare cover glass and TiO_2 NPs-coated cover glass, respectively. Figure 2C displays the fluorescence emission trajectories of *m*-ZnTCPP on bare cover glass, which shows a nearly constant level of fluorescence intensity before photobleaching occurs. Parts D, F, and H of Figure 2 show fluorescence emission trajectories of *m*-ZnTCPP on TiO_2 NPs-coated cover glass, which show strong fluctuations and blinking between bright and dark states (histograms of the emission intensity in Figure 2E,G,I are shown to determine the threshold for dark and bright states) as opposed to a relatively stable emission on bare cover glass. For higher level emission intensity we have used the term "bright" and for lower level emission intensity we have used the term "dark", because in all of the fluorescence emission trajectories lower level emission intensity is almost equal to the background level (Figure S3 of Supporting Information). Similar single-molecule fluorescence intensity fluctuation and blinking between bright and dark states were also observed in our previous works on Coumarin 343−TiO_2,[9] *p*-ZnTCPP−TiO_2,[79] and PF−TiO_2.[80]

We recorded the fluorescence emission trajectories of more than 100 molecules of *m*-ZnTCPP on TiO_2 NP-coated cover glass. The single-molecule fluorescence time trajectories have the essential feature of blinking between the bright states and the dark states. In our previous reports,[9,79,80] we have determined that the blinking behavior is predominately a consequence of the fluctuating interfacial electron transfer rate, and for each intensity bin of a few milliseconds, multiple electron transfer events occur and interfacial ET results in a dark state of the molecules. For each photoexcitation, the excited state of the single-molecule either undergoes radiative emission to yield a photon that contributes to a bright state or undergoes a nonradiative electron transfer process that contributes to the dark state (Figure 3). The ratio between the radiative and nonradiative rate processes, ultimately determined by the radiative rate of approximately nanoseconds vs the nonradiative rate of shorter than nanosecond down to femtoseconds that is regulated by the coupling between the molecule and the substrate.

The trend of fluorescence emission trajectories of single molecules shows about 70% of the molecules follow the trace dominated by the dark state as shown in Figure 2D, and 10−20% of the molecules follow the trace where dominance of the dark state is less prominent (such as the traces shown in Figure

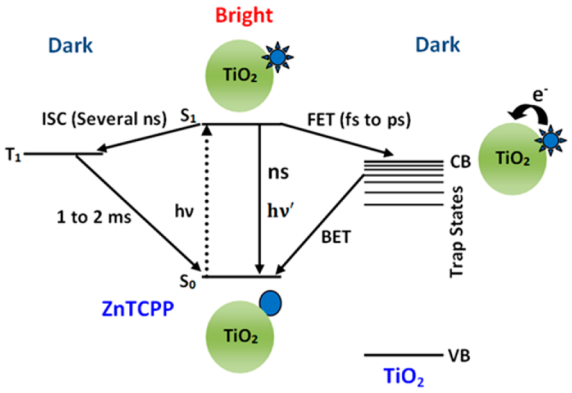

Figure 3. Schematic diagram showing energy levels and photoinduced processes involved in the ZnTCPP−TiO_2 system: CB, conduction band; VB, valence band; ISC, intersystem crossing. In the ZnTCPP−TiO_2 system the photoexcited single-molecule either involves radiative emission to yield a photon that contributes to a bright state or involves a nonradiative electron transfer process that contributes to the dark state.

2F,H). For the majority of the molecules, the dark state is dominant in their single-molecule fluorescence trajectories, which indicates strong interaction of *m*-ZnTCPP with TiO_2 compared to that of *p*-ZnTCPP where the dark state is significantly less dominating.[79] Evidently, *m*-ZnTCPP on TiO_2 has more active electron transfer such that the fluorescence process is suppressed. This difference in the behavior of *m*-ZnTCPP and *p*-ZnTCPP can be accounted for by the difference in the binding mode (Figure 1), hence the electronic coupling between the adsorbed molecules and TiO_2. Another possible explanation could have been attributed to the different ground-state electronic nature of *m*-ZnTCPP and *p*-ZnTCPP. However, the position of the carboxyl anchoring groups has little influence in the ground-state electronic nature of the molecule, because of the orthogonal orientation of the *meso*-phenyl rings of the porphyrin macrocycle, evidenced by similar absorption spectra of the *m*-ZnTCPP and *p*-ZnTCPP.[40]

Following our earlier study on interfacial electron transfer dynamics of *p*-ZnTCPP on TiO_2,[79] it can be said that the fluctuation of fluorescence is not due to the rotation or translational motions of the single molecules. The covalently anchored molecules through multiple carboxylic groups do not have the flexibility of rotational or translation motions.[79] Additionally, the long dark time (Figures 2D,F,H) certainly shows that the fluctuation of fluorescence is not due to the triplet state, because the triplet-state lifetime of ZnTCPP dye lies close to 1 ms.[83] Therefore, we can conclude that the dark states in fluorescence intensity trajectories of *m*-ZnTCPP on TiO_2 originate due to the high ET reactivity, which quench the S_1-S_0 radiative emission, and the bright states originate due to the low ET reactivity leaving the S_1-S_0 radiative emission dominant, the same conclusion as we reported for the *p*-ZnTCPP on TiO_2.[9,79]

For further understanding about the ET reactivity fluctuation and to explain the observed difference in the behavior of *m*-ZnTCPP and *p*-ZnTCPP, we measured fluorescence lifetimes of single molecules using single-molecule photon-stamping spectroscopy (Figure 4). Figure 4A shows the fluorescence emission trajectory of *m*-ZnTCPP on TiO_2 NPs-coated cover glass, and Figure 4B shows a histogram of the emission intensity to determine the threshold for dark and bright states. To determine the threshold for dark and bright states, the average background level (after the photobleaching step) and its standard deviation σ were determined first and then the threshold was defined typically at 3σ higher than the average background level. The fluorescence emission trajectory of Figure 4A is separated to higher level emission (marked as 1) and lower level emission (marked as 2) based on a threshold of 77 photon counts/(50 ms). In single-molecule photon-stamping measurement, for each detected photon (each data point in Figure 4C,E represents a detected photon) two parameters were recorded: chronic arrival time (*x*-axis of Figure 4C,E) and delay time between the laser pulse excitation and the photon emission from the excited state (*y*-axis of Figure 4C,E). The histograms of chronic arrival times yield fluorescence intensity trajectories with a given time bin resolution, and the distribution of the delay times give a typical single-molecule fluorescence decay curve.[9,79,80] The single-molecule fluorescence lifetime was analyzed for both the higher level emission intensity and lower level emission intensity.

Parts C, E, and D, F of Figure 4 show the photon-stamping data including chronic arrival time and delay time for each photon, and corresponding histograms respectively, for a typical bright state (in blue, 9.0−10.0 s) and dark state (in red, 7.5−8.5 s). The distributions of delay times of these two typical blinking states are different. The lifetime analysis for higher level emission and lower level emission of the whole trajectory is shown in Figure 4G,H, respectively. These single-molecule fluorescence decay curves were derived from the distribution of the delay times for higher level emission's and lower level emission's photon-stamping data of the whole trajectory. The lifetime derived from the higher level emission intensity shows 3.48 times longer lifetime (3.90 ± 0.15 ns) than the lifetime derived from the lower level emission intensity (1.12 ± 0.10 ns). These observations clearly indicate that the fluorescence quenching is the result of FET from the excited state of the adsorbate *m*-ZnTCPP to the TiO_2 NPs. The emission intensity fluctuations further demonstrate the ET reactivity fluctuation.

For *p*-ZnTCPP on TiO_2, the lifetime derived from the higher level emission intensity is nearly similar to the lifetime derived from the lower level emission intensity.[79] Contrastingly, *m*-ZnTCPP on TiO_2 shows 3.48 times shorter lifetime in the case of lower level emission intensity when the ET activity is high compared to the lifetime derived from the higher level emission intensity when the radiative emission is dominated and ET activity is low. These observations suggest greater charge injection efficiency of *m*-ZnTCPP compared to the *p*-ZnTCPP. The difference in the ET activity of *m*-ZnTCPP and *p*-ZnTCPP can be accounted for by the difference in the binding mode (Figure 1): the four anchoring groups (COOH) in the meta-position of the *meso*-phenyl rings of the porphyrin macrocycle of *m*-ZnTCPP favors a planar binding mode to the TiO_2 surface,[40,86,88] decreasing the distance between the molecule transition dipole and TiO_2 surface, which in turn favors the greater electronic coupling between the molecule and TiO_2 as well as the charge injection efficiency. The greater charge injection efficiency with the decreasing distance between the sensitizer and TiO_2 surface is well supported by earlier reports, where it has been shown that the ET rate decays exponentially with the increasing bridge length between sensitizer and TiO_2 surface.[98−100] The molecular motions or the flexibility of the adsorbed molecule on the semiconductor surface also influences the electronic coupling and, thus, the ET

dx.doi.org/10.1021/jp506199w | J. Phys. Chem. C 2014, 118, 20209−20221

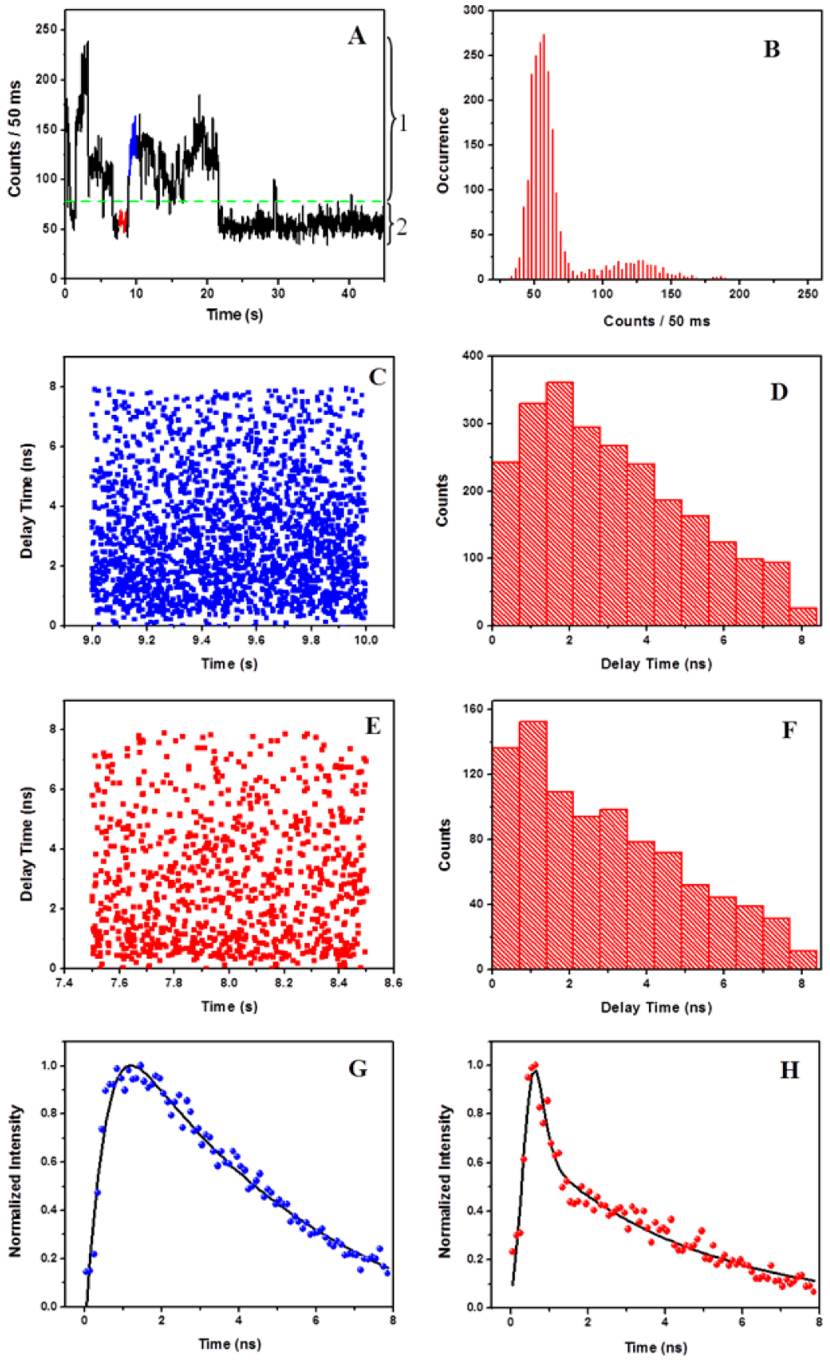

Figure 4. Single-molecule fluorescence decay profile of *m*-ZnTCPP on a TiO_2 NP surface. The fluorescence emission trajectory of *m*-ZnTCPP on TiO_2 NPs-coated cover glass and histogram of the emission intensity are displayed in A and B. Using 77 photon counts/(50 ms) as the threshold, the fluorescence emission trajectory is separated into higher level emission (marked as 1) and lower level emission (marked as 2). Panels C, E and D, F show the photon-stamping data and corresponding histogram for a typical bright state (in "blue", 9.0−10.0 s) and dark state (in "red", 7.5−8.5 s). The fluorescence decay profiles of higher level emission and lower level emission of the whole trajectory are displayed in G and H. The fit to the decay profiles (solid line) shown in G and H are biexponential fits derived by deconvolution of the instrument response function (IRF).

dynamics.[101] The four covalent anchor points of *m*-ZnTCPP compared to that of one or two covalent anchor points in the case of *p*-ZnTCPP[40,86,88] are expected to pose greater restriction on the movement of *m*-ZnTCPP than *p*-ZnTCPP. Therefore, the higher restrictive motion of *m*-ZnTCPP on TiO_2 NP surface can also be considered responsible for the greater charge injection efficiency compared to that of *p*-ZnTCPP.

Although we are not able to measure the ultrafast FET directly by single-molecule experiments in this work, the fluctuation in ET reactivity is well reflected in fluorescence emission trajectories and lifetime analysis of single molecules. Fluctuations in ET reactivity at different time points cause fluorescence blinking in individual molecules. That is why these molecules can still be observed by single-molecule imaging at single-photon counting sensitivity. The visibility of single molecules indicates that the FET time apparently fluctuates in a wide time scale from femtoseconds to nanoseconds or even slower. Had the time scale of the nonradiative decay (FET)

dx.doi.org/10.1021/jp506199w | J. Phys. Chem. C 2014, 118, 20209−20221

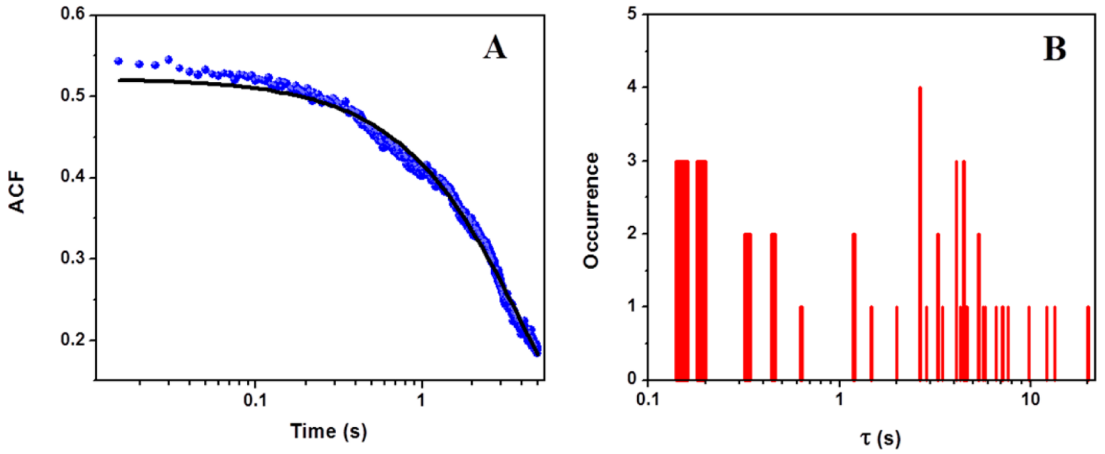

Figure 5. (A) Autocorrelation function (ACF) trace calculated from single-molecule fluorescence intensity time trajectory of *m*-ZnTCPP on TiO_2 NP surface. (B) Histogram of ACF decay times (τ), for 23 different molecules of *m*-ZnTCPP on TiO_2 NP surface.

been in the femtosecond to picosecond range only, the excited-state radiative emission efficiency should have been as low as 10^{-3} to 10^{-6} and the single molecules should be essentially nonfluorescent or not observable by photon detection. Here, it is also important to mention that in all our measurements we only consider those molecules which are visible. It is also interesting to note that the highly inhomogeneous interfacial electron transfer processes are widely noticeable in the ensemble-averaged time-resolved data in the literature; for example, there often is a long background in the time-resolved spectroscopic data that indicates a measurable amount of photons emitted through a slow radiative or nonradiative excited-state process at even nanosecond time scale.[100] Nevertheless, the ET does not always dominate the excited-state process of the *m*-ZnTCPP−TiO_2 system. In fact, single-molecule interfacial ET processes in *m*-/*p*-ZnTCPP−TiO_2 systems were found to be inhomogeneous, both dynamically and statically. The static inhomogeneity is associated with the difference observed in interfacial ET reactivity fluctuation from molecule to molecule, whereas the dynamic inhomogeneity is associated with the difference observed in interfacial ET reactivity fluctuation from time to time for a same individual molecule.

To further understand the ET reactivity fluctuation, we calculated the autocorrelation functions, $C(t)$, of the single-molecule fluorescence intensity trajectories. The autocorrelation function (ACF) is defined as

$$C(t) = \langle (I(0) - \langle I \rangle)(I(t) - \langle I \rangle) \rangle / \langle (I(0) - \langle I \rangle)^2 \rangle$$

where $I(0)$ and $I(t)$ represent the fluorescence intensity (photon count) of single-molecule fluorescence intensity trajectories at time zero and at time t, respectively, and $\langle I \rangle$ is the mean of the intensities of single-molecule fluorescence intensity trajectories.

Similar to our earlier studied Coumarin 343−TiO_2[9] and *p*-ZnTCPP−TiO_2[79] systems, the autocorrelation functions show nonexponential decays, which indicate the dynamic disorder of the interfacial ET reactivity; i.e., the fluctuation rate changes with time. The autocorrelation functions (Figure 5A) were fitted using biexponential functions with autocorrelation function decay time ranging from subseconds to seconds (Figure 5B). The biexponential fit to the autocorrelation function can be accounted for by the presence of two distinct states for all visible molecules: (i) the state in which the dye molecule interacts strongly with the TiO_2 surface leading to higher interfacial ET reactivity and the dark state; (ii) the state in which the dye molecule interacts weakly with the TiO_2 surface leading to lower interfacial ET reactivity and the bright state. Figure 5B shows the histogram of autocorrelation function decay times (τ), for 23 different molecules of *m*-ZnTCPP on TiO_2 NP surface.

The distribution of autocorrelation function decay times for *m*-ZnTCPP molecules shows that the decay times for most molecules lie between 1 and 6 s, whereas in the case of *p*-ZnTCPP most molecules exhibit decay times between 0.1 and 0.4 s (the histogram of τ for *p*-ZnTCPP on TiO_2 NP surface is displayed in Figure S4 of the Supporting Information).[79] So, following the definition of autocorrelation function decay time, we can say that *m*-ZnTCPP shows a lower interfacial ET fluctuation rate than *p*-ZnTCPP. This difference can be again accounted for by the fact that the four covalent anchor points of *m*-ZnTCPP compared to that of one or two covalent anchor points in the case of *p*-ZnTCPP (Figure 1) poses greater restriction to the movement of *m*-ZnTCPP than *p*-ZnTCPP, which in turn causes a lower interfacial ET fluctuation rate in the case of *m*-ZnTCPP than *p*-ZnTCPP.

To quantify the emission intermittency recorded by the blinking single-molecule fluorescence trajectories, we performed statistical analysis on the stochastic durations of the dark state involving high ET reactivity compared to the bright state associated with low ET reactivity. The single-molecule fluorescence emission trajectories are used to determine the distribution of dark-time durations (vide supra). Parts A and B of Figure 6 show the distributions of dark-time durations of *m*-ZnTCPP on the TiO_2 NP surface for 1 molecule and 23 molecules, respectively. Broad ranges of blinking time scales, ranging over the temporal resolution of the experiment (1 ms) to seconds. The frequency of events (occurrence) is high with t_{dark} near the minimum integration bin width, whereas the occurrences become less dense at longer times. We observed non-Poisson behavior for *m*-ZnTCPP as indicated by the nonexponential distribution of dark times (Figure 6A,B), which suggests that the intrinsic physical mechanism is not originated from a single Poisson event under an exponential rate dynamics; rather it is the result of a complex rate process where the rate of ET changes from time to time.[9,79,102−105] The observed non-Poisson behavior for *m*-ZnTCPP is consistent with our previous findings with *p*-ZnTCPP.[79]

dx.doi.org/10.1021/jp506199w | J. Phys. Chem. C 2014, 118, 20209−20221

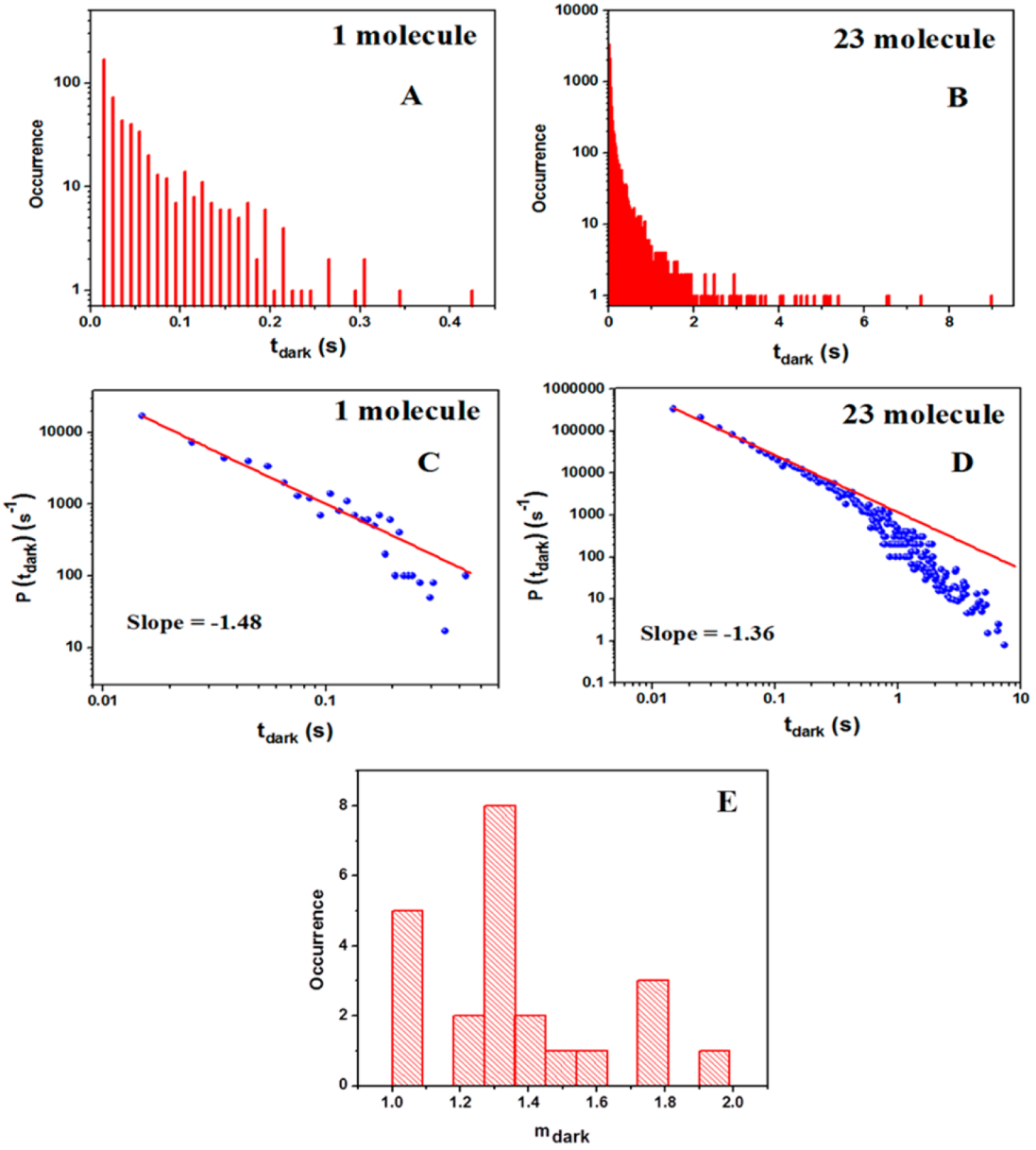

Figure 6. Distributions of dark-time durations of *m*-ZnTCPP on the TiO_2 NP surface for (A) 1 molecule and (B) 23 molecules. Probability densities of the dark-time durations of *m*-ZnTCPP on TiO_2 NP surface for (C) 1 molecule and (D) 23 molecules. In log−log scale plots (C, D) the solid lines are linear fits indicating power-law behavior. The power-law exponent, which is the slope of the linear fits, is also indicated in the panels. (E) Histogram of power-law exponents (m_{dark}), for 23 different molecules of *m*-ZnTCPP on the TiO_2 NP surface.

To further analyze the ET reactivity fluctuation associated with non-Poisson behavior, we generated probability density distribution of the dark states ($P(t_{dark})$ = occurrence$(t)/\Delta t$; Figure 6C,D).[106−111] Each data point of the histogram is weighted by the average time between the nearest neighbor events. The probability density built from different dark times show linear dependence on t_{dark} in log−log plots (Figure 6C,D). This linear dependence of the single-molecule dark-time probability density distributions shows typical power-law behavior, which can be mathematically described as $P(t_{dark}) \propto t_{dark}^{-m_{dark}}$. The slopes of the lines in Figure 6C,D give the values of power-law exponent m_{dark} for 1 molecule and 23 molecules, respectively. The observed power-law kinetics is also consistent with our earlier results.[79] Several models exist that explain the power-law blinking behavior of single molecules on semiconductor surfaces.[107−111] Following our earlier studied system[79] we can say that power-law blinking of the organic molecule requires dynamic disorder dynamics.[103] The observed power-law statistical behavior, being intrinsically derived from the interfacial ET dynamics, reflects the dynamic disorder of the ET reactivity.

In Figure 6E we show the distribution of the power-law exponents, m_{dark}, for 23 molecules. The value of m_{dark} varies from 1.00 to 1.99, indicating a large spread in dark-time behavior from molecule to molecule, which in turn reflects the static inhomogeneity of the ET reactivity fluctuation. The larger spread of m_{dark} in the case of *p*-ZnTCPP (1.02−2.68) than that of *m*-ZnTCPP (1.00−1.99) again supports the higher flexibility of *p*-ZnTCPP on the TiO_2 surface (the histogram of m_{dark} for *p*-ZnTCPP on the TiO_2 NP surface is displayed in Figure S5 of Supporting Information). In addition to this the lower mean value of m_{dark} in the case of *m*-ZnTCPP (1.35) than *p*-ZnTCPP

dx.doi.org/10.1021/jp506199w | J. Phys. Chem. C 2014, 118, 20209−20221

(1.79)[79] indicates a relatively higher probability for large dark times in the case of *m*-ZnTCPP than *p*-ZnTCPP. Therefore, according to our earlier discussions, a higher probability for large dark times in the case of *m*-ZnTCPP than that of *p*-ZnTCPP reflects the higher ET reactivity of *m*-ZnTCPP than *p*-ZnTCPP.

The preceding discussion attests to the fact that both the autocorrelation function decay time and m_{dark} are critical factors for the analysis of interfacial ET reactivity fluctuation dynamics. τ provides useful information about the ET reactivity fluctuation time, and the specific value of τ gives a statistical estimate of the time scale fluctuation for a single molecule alternating between bright and dark states. m_{dark} indicates the relative probability for the dark-state durations: a larger m_{dark} value indicates a relatively higher probability for small dark times compared to larger dark times. Both the autocorrelation function decay time and m_{dark} are found to be sensitive to the molecular structure (different for *m*-ZnTCPP and *p*-ZnTCPP) and/or molecular environment. The structural change of the dye molecule from *p*-ZnTCPP to *m*-ZnTCPP is always accompanied by the change in electrostatic and hydrophobic interactions between the probe molecules and their fluctuating local environment[75,112,113] leading to the difference in interfacial ET reactivity. The conclusions derived from ensemble-averaged measurement and single-molecule measurement are consistent, but the sensitivity about (i) inhomogeneous interfacial ET reactivity fluctuation, (ii) the broad range of autocorrelation function decay time, and (iii) the inherent broadness of the power-law exponent may remain hidden by ensemble-averaged measurements.

Overall, the observed differences in the interfacial electron transfer reactivity of *m*-ZnTCPP and *p*-ZnTCPP can be associated with the difference in the redox reactivity intermittency with the fluctuation of molecule−TiO_2 electronic and Franck−Condon coupling. In fact, the difference in the inhomogeneous surface-state distribution of *m*-ZnTCPP and *p*-ZnTCPP molecules plays a critical role in the electronic coupling parameter. Specifically, the formation stability and rupture of four anchoring groups of the *m*-ZnTCPP to TiO_2 compared to that of one or two anchoring groups of the *p*-ZnTCPP to TiO_2 may produce the difference in the extent of perturbed electronic coupling by local environment thermal fluctuation at room temperature.[9,114−117] Understanding the role of dye molecule−semiconductor interaction on interfacial ET is central to the development of solar energy conversion science and photocatalysis. However, the quantification of electronic coupling is challenging because of the inherent heterogeneity and the involvement of different factors affecting electronic coupling. Depending on the strength of electronic coupling between the excited state of the sensitizer and the acceptor orbitals at the surface of TiO_2, the interfacial ET process was reported to take place on time scales ranging from less than 10 fs to several microseconds.[100,118] Nevertheless, the strong electronic coupling is often the result of the anchoring of the dye molecule onto the semiconductor surface through a moiety carrying its LUMO.[100] Considering the separation distance between *m*-ZnTCPP/*p*-ZnTCPP and the TiO_2 surface as the only factor determining the magnitude of electronic coupling for interfacial ET, we can use the Gamov expression[100]

$$|H|^2 = |H_0|^2 \exp[-\beta(r - r_0)]$$

where $|H|$ and $|H_0|$ are electronic coupling between donor and acceptor at separation distances r and r_0, respectively, and β is the damping factor (an exponential coefficient for the decay of the electronic wave function).[100] The change of sensitizer from *p*-ZnTCPP to *m*-ZnTCPP is accompanied by a decrease in the distance between donor (sensitizer) and acceptor,[40] which in turn causes greater electronic coupling in the case of *m*-ZnTCPP than *p*-ZnTCPP. Additionally, the change of sensitizer from *p*-ZnTCPP to *m*-ZnTCPP is also accompanied by an increase in the number of anchoring groups from 1or 2 in the case of *p*-ZnTCPP to 4 in the case of *m*-ZnTCPP,[40,86,88] which in turn decreases the flexibility of *m*-ZnTCPP compared to *p*-ZnTCPP. The diminished flexibility of *m*-ZnTCPP can further decrease the damping factor β leading to an increase in electronic coupling between *m*-ZnTCPP and TiO_2.[100,101]

This simplified picture is certainly not true because in a system gated with dye molecule on top of TiO_2 surface, the dye−TiO_2 electron coupling to vibrational modes of the dye molecule must be taken into consideration.[91] Specifically, at room temperature the local thermal fluctuation is significant enough to change and perturb the molecule−TiO_2 electron coupling to vibrational modes of the molecule. This also accords with our earlier observations, where we showed that for alizarin−TiO_2 interfaces the vibrational reorganization energy barriers of interfacial ET are inhomogeneous from TiO_2 nanoparticle to nanoparticle and from molecular site to site.[91] Some of the issues emerging from this finding, such as broad fluctuation subspace of the electronic coupling factor, relate specifically to the broad range of autocorrelation function decay time and the inherent broadness of the power-law exponent. The conclusions derived from this study are consistent with the findings of extensive literature on ensemble-averaged measurements, which suggest that the inhomogeneous interfacial ET arises due to the surface defects, changes in electronic coupling, changes in the distance between donor and acceptor, and multiple time scale of energetic relaxation and solvation dynamics.[19−22,119−122] The combination of our findings reveals partially the origin of the complexity of the interfacial ET dynamics. However, more research on this topic needs to be undertaken before the quantification of the inhomogeneous interfacial ET dynamics.

4. CONCLUSION

We studied interfacial ET dynamics of the *m*-ZnTCPP-TiO_2 nanoparticle system by applying single-molecule photon-stamping spectroscopy. Single-molecule fluorescence intensity fluctuations of *m*-ZnTCPP on TiO_2 NP surface are identified to have originated from the interfacial ET reactivity fluctuation. Similar to our earlier studied *p*-ZnTCPP-TiO_2 nanoparticle system, the single-molecule interfacial ET processes in *m*-ZnTCPP−TiO_2 systems were found to be inhomogeneous, both statically (molecule to molecule) and dynamically (time to time for the same individual molecules). The dominant dark states in single-molecule fluorescence intensity trajectories as well as a large difference in lifetime derived from bright and dark states of *m*-ZnTCPP on TiO_2 NP surface compared to that of *p*-ZnTCPP demonstrate higher charge injection efficiency of *m*-ZnTCPP than *p*-ZnTCPP. The change in four anchoring groups (-COOH group) position from para-position to meta-position of *meso*-phenyl rings of the porphyrin macrocycle produces changes in binding geometry, hence electronic coupling, which in turn facilitates interfacial ET reactivity. The higher charge injection efficiency of *m*-ZnTCPP

dx.doi.org/10.1021/jp506199w | J. Phys. Chem. C 2014, 118, 20209−20221

compared to *p*-ZnTCPP is explained by considering the shorter distance between the sensitizer (*m*-ZnTCPP) and the TiO_2 surface as well as the higher restrictive motion of the sensitizer (*m*-ZnTCPP) on the TiO_2 surface.

The nonexponential autocorrelation function decay and a large spread in power-law exponent, m_{dark}, derived from single-molecule fluorescence intensity trajectories reflect inhomogeneous interfacial ET dynamics. The analysis of autocorrelation function decay time and m_{dark} show different behaviors of *m*-ZnTCPP and *p*-ZnTCPP, which indicates the sensitivity of τ and m_{dark} on the molecular structure and molecular environment of the dye molecule.

Our single-molecule study provides detailed molecular level understanding of the inhomogeneous interfacial ET reactivity and the factors influencing the ET reactivity. The molecular level understanding of the interfacial ET reactivity further sheds light on the intrinsic fluctuating and inhomogeneous interfacial electron transfer dynamics, which may, for example, help the development of solar energy conversion science and photocatalysis.

■ ASSOCIATED CONTENT

Supporting Information

Figures showing the control experiment for confocal fluorescence imaging, UV−vis absorption and fluorescence emission spectra of *m*-ZnTCPP, fluorescence emission trajectory showing the photobleaching step, and direct comparison between *m*-ZnTCPP and *p*-ZnTCPP data. This material is available free of charge via the Internet at http://pubs.acs.org.

■ AUTHOR INFORMATION

Corresponding Author

*E-mail: hplu@bgsu.edu. Tel.: 419-372-1840.

Notes

The authors declare no competing financial interests.

■ ACKNOWLEDGMENTS

This work is supported by the Office of Basic Energy Sciences within the Office of Science of the U.S. Department of Energy (DOE).

■ REFERENCES

(1) Reisner, E.; Powell, D. J.; Cavazza, C.; Fontecilla-Camps, J. C.; Armstrong, F. A. Visible Light-Driven H_2 Production by Hydrogenases Attached to Dye-Sensitized TiO_2 Nanoparticles. *J. Am. Chem. Soc.* **2009**, *131*, 18457−18466.

(2) Chen, Y. S.; Kamat, P. V. Glutathione-Capped Gold Nanoclusters as Photosensitizers. Visible Light-Induced Hydrogen Generation in Neutral Water. *J. Am. Chem. Soc.* **2014**, *136*, 6075−6082.

(3) Fabregat-Santiago, F.; Bisquert, J.; Palomares, E.; Otero, L.; Kuang, D.; Zakeeruddin, S. M.; Grätzel, M. Correlation between Photovoltaic Performance and Impedance Spectroscopy of Dye-Sensitized Solar Cells Based on Ionic Liquids. *J. Phys. Chem. C* **2007**, *111*, 6550−6560.

(4) Ardo, S.; Achey, D.; Morris, A. J.; Abrahamsson, M.; Meyer, G. J. Non-Nernstian Two-Electron Transfer Photocatalysis at Metalloporphyrin−TiO_2 Interfaces. *J. Am. Chem. Soc.* **2011**, *133*, 16572−16580.

(5) Song, W.; Ito, A.; Binstead, R. A.; Hanson, K.; Luo, H.; Brennaman, M. K.; Concepcion, J. J.; Meyer, T. J. Accumulation of Multiple Oxidative Equivalents at a Single Site by Cross-Surface Electron Transfer on TiO_2. *J. Am. Chem. Soc.* **2013**, *135*, 11587−11594.

(6) Balasubramanian, S.; Wang, P.; Schaller, R. D.; Rajh, T.; Rozhkova, E. A. High-Performance Bioassisted Nanophotocatalyst for Hydrogen Production. *Nano Lett.* **2013**, *13*, 3365−3371.

(7) Koops, S. E.; O'Regan, B. C.; Barnes, P. R. F.; Durrant, J. R. Parameters Influencing the Efficiency of Electron Injection in Dye-Sensitized Solar Cells. *J. Am. Chem. Soc.* **2009**, *131*, 4808−4818.

(8) Zhu, K.; Neale, N. R.; Miedaner, A.; Frank, A. J. Enhanced Charge-Collection Efficiencies and Light Scattering in Dye-Sensitized Solar Cells Using Oriented TiO_2 Nanotubes Arrays. *Nano Lett.* **2007**, *7*, 69−74.

(9) Biju, V.; Micic, M.; Hu, D.; Lu, H. P. Intermittent Single-Molecule Interfacial Electron Transfer Dynamics. *J. Am. Chem. Soc.* **2004**, *126*, 9374−9381.

(10) Li, B.; Zhao, J.; Onda, K.; Jordan, K. D.; Yang, J. L.; Petek, H. Ultrafast Interfacial Proton-Coupled Electron Transfer. *Science* **2006**, *311*, 1436−1440.

(11) Lee, J. K.; Ma, W. L.; Brabec, C. J.; Yuen, J.; Moon, J. S.; Kim, J. Y.; Lee, K.; Bazan, G. C.; Heeger, A. J. Processing Additives for Improved Efficiency from Bulk Heterojunction Solar Cells. *J. Am. Chem. Soc.* **2008**, *130*, 3619−3623.

(12) Park, Y.; Kim, W.; Monllor-Satoca, D.; Tachikawa, T.; Majima, T.; Choi, W. Role of Interparticle Charge Transfers in Agglomerated Photocatalyst Nanoparticles: Demonstration in Aqueous Suspension of Dye-Sensitized TiO_2. *J. Phys. Chem. Lett.* **2013**, *4*, 189−194.

(13) Kamat, P. V. Manipulation of Charge Transfer Across Semiconductor Interface. A Criterion That Cannot Be Ignored in Photocatalyst Design. *J. Phys. Chem. Lett.* **2012**, *3*, 663−672.

(14) Akimov, A. V.; Neukirch, A. J.; Prezhdo, O. V. Theoretical Insights into Photoinduced Charge Transfer and Catalysis at Oxide Interfaces. *Chem. Rev.* **2013**, *113*, 4496−4565.

(15) Zhao, Y.; Swierk, J. R.; Megiatto, J. D., Jr.; Sherman, B.; Youngblood, W. J.; Qin, D.; Lentz, D. M.; Moore, A. L.; Moore, T. A.; Gust, D.; Mallouk, T. E. Improving the Efficiency of Water Splitting in Dye-Sensitized Solar Cells by Using a Biomimetic Electron Transfer Mediator. *Proc. Natl. Acad. Sci. U. S. A.* **2012**, *109*, 15612−15616.

(16) Shahzad, N.; Risplendi, F.; Pugliese, D.; Bianco, S.; Sacco, A.; Lamberti, A.; Gazia, R.; Tresso, E.; Cicero, G. Comparison of Hemi-Squaraine Sensitized TiO_2 and ZnO Photoanodes for DSSC Applications. *J. Phys. Chem. C* **2013**, *117*, 22778−22783.

(17) Hamada, M.; Takenokoshi, N.; Matozaki, K.; Feng, Q.; Murase, N.; Wakida, S.; Nakanishi, S.; Biju, V. In Situ Photochemical Surface Passivation of CdSe/ZnS Quantum Dots for Quantitative Light Emission and Enhanced Photocurrent Response in Solar Cells. *J. Phys. Chem. C* **2014**, *118*, 2178−2186.

(18) Burke, A.; Ito, S.; Snaith, H.; Bach, U.; Kwiatkowski, J.; Grätzel, M. The Function of a TiO_2 Compact Layer in Dye-Sensitized Solar Cells Incorporating "Planar" Organic Dyes. *Nano Lett.* **2008**, *8*, 977−981.

(19) Anderson, N. A.; Lian, T. Q. Ultrafast Electron Transfer at the Molecule-Semiconductor Nanoparticle Interface. *Annu. Rev. Phys. Chem.* **2005**, *56*, 491−519.

(20) Duncan, W. R.; Prezhdo, O. V. Theoretical Studies of Photoinduced Electron Transfer in Dye-Sensitized TiO_2. *Annu. Rev. Phys. Chem.* **2007**, *58*, 143−184.

(21) Watson, D. F.; Meyer, G. J. Electron Injection at Dye-Sensitized Semiconductor Electrodes. *Annu. Rev. Phys. Chem.* **2005**, *56*, 119−156.

(22) Wenger, B.; Grätzel, M.; Moser, J.-E. Rationale for Kinetic Heterogeneity of Ultrafast Light-Induced Electron Transfer from Ru(II) Complex Sensitizers to Nanocrystalline TiO_2. *J. Am. Chem. Soc.* **2005**, *127*, 12150−12151.

(23) Feng, X.; Zhu, K.; Frank, A. J.; Grimes, C. A.; Mallouk, T. E. Rapid Charge Transport in Dye-Sensitized Solar Cells Made from Vertically Aligned Single-Crystal Rutile TiO_2 Nanowires. *Angew. Chem., Int. Ed.* **2012**, *51*, 2727−2730.

(24) Park, Y.; Kim, W.; Monllor-Satoca, D.; Tachikawa, T.; Majima, T.; Choi, W. Role of Interparticle Charge Transfers in Agglomerated Photocatalyst Nanoparticles: Demonstration in Aqueous Suspension of Dye-Sensitized TiO_2. *J. Phys. Chem. Lett.* **2013**, *4*, 189−194.

(25) De Angelis, F.; Fantacci, S.; Selloni, A.; Nazeeruddin, M. K.; Grätzel, M. Time-Dependent Density Functional Theory Investigations on the Excited States of Ru(II)-Dye-Sensitized TiO_2 Nanoparticles: The Role of Sensitizer Protonation. *J. Am. Chem. Soc.* **2007**, *129*, 14156−14157.
(26) Duncan, W. R.; Stier, W. M.; Prezhdo, O. V. *Ab Initio* Nonadiabatic Molecular Dynamics of the Ultrafast Electron Injection across the Alizarin−TiO_2 Interface. *J. Am. Chem. Soc.* **2005**, *127*, 7941−7951.
(27) Yanagida, S.; Yu, Y.; Manseki, K. Iodine/Iodide-Free Dye-Sensitized Solar Cells. *Acc. Chem. Res.* **2009**, *42*, 1827−1838.
(28) Li, J.; Kondov, I.; Wang, H.; Thoss, M. Theoretical Study of Photoinduced Electron-Transfer Processes in the Dye−Semiconductor System Alizarin−TiO_2. *J. Phys. Chem. C* **2010**, *114*, 18481−18493.
(29) Robson, K. C. D.; Hu, K.; Meyer, G. J.; Berlinguette, C. P. Atomic Level Resolution of Dye Regeneration in the Dye-Sensitized Solar Cell. *J. Am. Chem. Soc.* **2013**, *135*, 1961−1971.
(30) Johansson, P. G.; Kopecky, A.; Galoppini, E.; Meyer, G. J. Distance Dependent Electron Transfer at TiO_2 Interfaces Sensitized with Phenylene Ethynylene Bridged Ru^{II}−Isothiocyanate Compounds. *J. Am. Chem. Soc.* **2013**, *135*, 8331−8341.
(31) Ye, S.; Kathiravan, A.; Hayashi, H.; Tong, Y.; Infahsaeng, Y.; Chabera, P.; Pascher, T.; Yartsev, A. P.; Isoda, S.; Imahori, H.; Sundström, V. Role of Adsorption Structures of Zn-Porphyrin on TiO_2 in Dye-Sensitized Solar Cells Studied by Sum Frequency Generation Vibrational Spectroscopy and Ultrafast Spectroscopy. *J. Phys. Chem. C* **2013**, *117*, 6066−6080.
(32) Jeong, N. C.; Farha, O. K.; Hupp, J. T. A Convenient Route to High Area, Nanoparticulate TiO_2 Photoelectrodes Suitable for High-Efficiency Energy Conversion in Dye-Sensitized Solar Cells. *Langmuir* **2011**, *27*, 1996−1999.
(33) Robel, I.; Kuno, M.; Kamat, P. V. Size-Dependent Electron Injection from Excited CdSe Quantum Dots into TiO_2 Nanoparticles. *J. Am. Chem. Soc.* **2007**, *129*, 4136−4137.
(34) Luo, J.; Xu, M.; Li, R.; Huang, K.-W.; Jiang, C.; Qi, Q.; Zeng, W.; Zhang, J.; Chi, C.; Wang, P.; Wu, J. *N*-Annulated Perylene as an Efficient Electron Donor for Porphyrin-Based Dyes: Enhanced Light-Harvesting Ability and High-Efficiency Co(II/III)-Based Dye-Sensitized Solar Cells. *J. Am. Chem. Soc.* **2014**, *136*, 265−272.
(35) Moehl, T.; Tsao, H. N.; Wu, K.-L.; Hsu, H.-C.; Chi, Y.; Ronca, E.; Angelis, F. D.; Nazeeruddin, M. K.; Grätzel, M. High Open-Circuit Voltages: Evidence for a Sensitizer-Induced TiO_2 Conduction Band Shift in Ru(II)-Dye Sensitized Solar Cells. *Chem. Mater.* **2013**, *25*, 4497−4502.
(36) She, C.; Guo, J.; Irle, S.; Morokuma, K.; Mohler, D. L.; Zabri, H.; Odobel, F.; Youm, K. T.; Liu, F.; Hupp, J. T.; Lian, T. Comparison of Interfacial Electron Transfer through Carboxylate and Phosphonate Anchoring Groups. *J. Phys. Chem. A* **2007**, *111*, 6832−6842.
(37) Jin, S.; Snoeberger, R. C., III; Issac, A.; Stockwell, D.; Batista, V. S.; Lian, T. Single-Molecule Interfacial Electron Transfer in Donor-Bridge-Nanoparticle Acceptor Complexes. *J. Phys. Chem. B* **2010**, *114*, 14309−14319.
(38) Niu, H.; Zhang, S.; Wang, R.; Guo, Z.; Shang, X.; Gan, W.; Qin, S.; Wan, L.; Xu, J. Dye-Sensitized Solar Cells Employing a Multifunctionalized Hierarchical SnO_2 Nanoflower Structure Passivated by TiO_2 Nanogranulum. *J. Phys. Chem. C* **2014**, *118*, 3504−3513.
(39) Prasittichai, C.; Hupp, J. T. Surface Modification of SnO_2 Photoelectrodes in Dye-Sensitized Solar Cells: Significant Improvements in Photovoltage via Al_2O_3 Atomic Layer Deposition. *J. Phys. Chem. Lett.* **2010**, *1*, 1611−1615.
(40) Rochford, J.; Chu, D.; Hagfeldt, A.; Galoppini, E. Tetrachelate Porphyrin Chromophores for Metal Oxide Semiconductor Sensitization: Effect of the Spacer Length and Anchoring Group Position. *J. Am. Chem. Soc.* **2007**, *129*, 4655−4665.
(41) Lissau, J. S.; Gardner, J. M.; Morandeira, A. Photon Upconversion on Dye-Sensitized Nanostructured ZrO_2 Films. *J. Phys. Chem. C* **2011**, *115*, 23226−23232.
(42) Ramakrishna, G.; Singh, A. K.; Palit, D. K.; Ghosh, H. N. Dynamics of Interfacial Electron Transfer from Photoexcited Quinizarin (Qz) into the Conduction Band of TiO_2 and Surface States of ZrO_2 Nanoparticles. *J. Phys. Chem. B* **2004**, *108*, 4775−4783.
(43) Maity, P.; Debnath, T.; Akbar, A.; Verma, S.; Ghosh, H. N. Ultrafast Electron-Transfer and -Trapping Dynamics in the Inter-Band-Gap States of ZrO_2 Nanoparticles Sensitized by Baicalein. *J. Phys. Chem. C* **2013**, *117*, 17531−17539.
(44) Law, M.; Greene, L. E.; Johnson, J. C.; Saykally, R.; Yang, P. Nanowire Dye-Sensitized Solar Cells. *Nat. Mater.* **2005**, *4*, 455−459.
(45) Martinson, A. B. F.; Góes, M. S.; Fabregat-Santiago, F.; Bisquert, J.; Pellin, M. J.; Hupp, J. T. Electron Transport in Dye-Sensitized Solar Cells Based on ZnO Nanotubes: Evidence for Highly Efficient Charge Collection and Exceptionally Rapid Dynamics. *J. Phys. Chem. A* **2009**, *113*, 4015−4021.
(46) Yella, A.; Lee, H.-W.; Tsao, H. N.; Yi, C.; Chandiran, A. K.; Nazeeruddin, Md. K.; Diau, E. W.-G.; Yeh, C.-Y.; Zakeeruddin, S. M.; Grätzel, M. Porphyrin-Sensitized Solar Cells with Cobalt (II/III)-Based Redox Electrolyte Exceed 12% Efficiency. *Science* **2011**, *334*, 629−634.
(47) Mathew, S.; Yella, A.; Gao, P.; Baker, R. H.; Curchod, B. F. E.; Astani, N. A.; Tavernelli, I.; Rothlisberger, U.; Nazeeruddin, Md. K.; Grätzel, M. Dye-Sensitized Solar Cells with 13% Efficiency Achieved through the Molecular Engineering of Porphyrin Sensitizers. *Nat. Chem.* **2014**, *6*, 242−247.
(48) Hardin, B. E.; Snaith, H. J.; McGehee, M. D. The Renaissance of Dye-Sensitized Solar Cells. *Nat. Photonics* **2012**, *6*, 162−169.
(49) Grätzel, M. Recent Advances in Sensitized Mesoscopic Solar Cells. *Acc. Chem. Res.* **2009**, *42*, 1788−1798.
(50) O'Regan, B.; Grätzel, M. A Low-Cost, High-Efficiency Solar Cell Based on Dye-Sensitized Colloidal TiO_2 Films. *Nature* **1991**, *353*, 737−740.
(51) Hagfeldt, A.; Boschloo, G.; Sun, L. C.; Kloo, L.; Pettersson, H. Dye-Sensitized Solar Cells. *Chem. Rev.* **2010**, *110*, 6595−6663.
(52) deJongh, P. E.; Vanmaekelbergh, D. Trap-Limited Electronic Transport in Assemblies of Nanometer-Size TiO_2 Particles. *Phys. Rev. Lett.* **1996**, *77*, 3427−3430.
(53) Klafter, J.; Sokolov, I. M. Anomalous Diffusion Spreads Its Wings. *Phys. World* **2005**, *18*, 29−32.
(54) Banerjee, T.; Kaniyankandy, S.; Das, A.; Ghosh, H. N. Newly Designed Resorcinolate Binding for Ru(II)− and Re(I)−Polypyridyl Complexes on Oleic Acid Capped TiO_2 in Nonaqueous Solvent: Prolonged Charge Separation and Substantial Thermalized ^{3}MLCT Injection. *J. Phys. Chem. C* **2013**, *117*, 3084−3092.
(55) Ghosh, H. N.; Asbury, J. B.; Weng, Y. X.; Lian, T. Q. Interfacial Electron Transfer between $Fe(II)(CN)_6^{4-}$ and TiO_2 Nanoparticles: Direct Electron Injection and Nonexponential Recombination. *J. Phys. Chem. B* **1998**, *102*, 10208−10215.
(56) Weng, Y. X.; Wang, Y. Q.; Asbury, J. B.; Ghosh, H. N.; Lian, T. Q. Back Electron Transfer from TiO_2 Nanoparticles to $Fe^{III}(CN)_6^{3-}$: Origin of Non-Single-Exponential and Particle Size Independent Dynamics. *J. Phys. Chem. B* **2000**, *104*, 93−104.
(57) Lu, H.; Prieskorn, J. N.; Hupp, J. T. Fast Interfacial Electron Transfer: Evidence for Inverted Region Kinetic Behavior. *J. Am. Chem. Soc.* **1993**, *115*, 4927−4928.
(58) Haque, S. A.; Tachibana, Y.; Klug, D. R.; Durrant, J. R. Charge Recombination Kinetics in Dye-Sensitized Nanocrystalline Titanium Dioxide Films under Externally Applied Bias. *J. Phys. Chem. B* **1998**, *102*, 1745−1749.
(59) Kaniyankandy, S.; Verma, S.; Mondal, J. A.; Palit, D. K.; Ghosh, H. N. Evidence of Multiple Electron Injection and Slow Back Electron Transfer in Alizarin-Sensitized Ultrasmall TiO_2 Particles. *J. Phys. Chem. C* **2009**, *113*, 3593−3599.
(60) Nelson, J.; Chandler, R. E. Random Walk Models of Charge Transfer and Transport in Dye Sensitized Systems. *Coord. Chem. Rev.* **2004**, *248*, 1181−1194.
(61) Nelson, J.; Haque, S. A.; Klug, D. R.; Durrant, J. R. Trap-Limited Recombination in Dye-Sensitized Nanocrystalline Metal Oxide Electrodes. *Phys. Rev. B* **2001**, *63*, 205321-1−205321-9.

(62) Ziółek, M.; Cohen, B.; Yang, X.; Sun, L.; Paulose, M.; Varghese, O. K.; Grimes, C. A.; Douhal, A. Femtosecond to Millisecond Studies of Electron Transfer Processes in a Donor-(π-Spacer)-Acceptor Series of Organic Dyes for Solar Cells Interacting with Titania Nanoparticles and Ordered Nanotube Array Films. *Phys. Chem. Chem. Phys.* **2012**, *14*, 2816−2831.
(63) Imahori, H.; Kang, S.; Hayashi, H.; Haruta, M.; Kurata, H.; Isoda, S.; Canton, S. E.; Infahsaeng, Y.; Kathiravan, A.; Pascher, T.; Chábera, P.; Yartsev, A. P.; Sundström, V. Photoinduced Charge Carrier Dynamics of Zn−Porphyrin−TiO_2 Electrodes: The Key Role of Charge Recombination for Solar Cell Performance. *J. Phys. Chem. A* **2011**, *115*, 3679−3690.
(64) Matylitsky, V. V.; Dworak, L.; Breus, V. V.; Basché, T.; Wachtveitl, J. Ultrafast Charge Separation in Multiexcited CdSe Quantum Dots Mediated by Adsorbed Electron Acceptors. *J. Am. Chem. Soc.* **2009**, *131*, 2424−2425.
(65) Stockwell, D.; Yang, Y.; Huang, J.; Anfuso, C.; Huang, Z.; Lian, T. Comparison of Electron-Transfer Dynamics from Coumarin 343 to TiO_2, SnO_2, and ZnO Nanocrystalline Thin Films: Role of Interface-Bound Charge-Separated Pairs. *J. Phys. Chem. C* **2010**, *114*, 6560−6566.
(66) VandenBout, D. A.; Yip, W. T.; Hu, D. H.; Fu, D. K.; Swager, T. M.; Barbara, P. F. Discrete Intensity Jumps and Intramolecular Electronic Energy Transfer in the Spectroscopy of Single Conjugated Polymer Molecules. *Science* **1997**, *277*, 1074−1077.
(67) Yan, S. G.; Lyon, L. A.; Lemon, B. I.; Preiskorn, J. S.; Hupp, J. T. Energy Conversion Chemistry: Mechanisms of Charge Transfer at Metal-Oxide Semiconductor/Solution Interfaces. *J. Chem. Educ.* **1997**, *74*, 657−662.
(68) Myers, A. B. Resonance Raman Intensity Analysis of Excited-State Dynamics. *Acc. Chem. Res.* **1997**, *30*, 519−527.
(69) Hupp, J. T.; Williams, R. D. Using Resonance Raman Spectroscopy To Examine Vibrational Barriers to Electron Transfer and Electronic Delocalization. *Acc. Chem. Res.* **2001**, *34*, 808−817.
(70) Hilczer, M.; Tachiya, M. Stochastic Approach to Charge Separation in Multiexcited Quantum Dots. *J. Phys. Chem. C* **2009**, *113*, 18451−18454.
(71) Barbara, P. F. Single-Molecule Spectroscopy. *Acc. Chem. Res.* **2005**, *38*, 503−503.
(72) Holman, M. W.; Liu, R. C.; Adams, D. M. Single-Molecule Spectroscopy of Interfacial Electron Transfer. *J. Am. Chem. Soc.* **2003**, *125*, 12649−12654.
(73) Betzig, E.; Chichester, R. J. Single Molecules Observed by Near-Field Scanning Optical Microscopy. *Science* **1993**, *262*, 1422−1425.
(74) Xie, X. S.; Dunn, R. C. Probing Single Molecule Dynamics. *Science* **1994**, *265*, 361−364.
(75) Lu, H. P.; Xie, X. S. Single-Molecule Spectral Fluctuations at Room Temperature. *Nature* **1997**, *385*, 143−146.
(76) Palacios, R. E.; Fan, F.-R.; Grey, J. K.; Suk, J.; Bard, A. J.; Barbara, P. F. Charging and Discharging of Single Conjugated-Polymer Nanoparticles. *Nat. Mater.* **2007**, *6*, 680−685.
(77) Palacios, R. E.; Fan, F.-R.; Bard, A. J.; Barbara, P. F. Single-Molecule Spectroelectrochemistry (SMS-EC). *J. Am. Chem. Soc.* **2006**, *128*, 9028−9029.
(78) Moerner, W. E.; Orrit, M. Illuminating Single Molecules in Condensed Matter. *Science* **1999**, *283*, 1670−1676.
(79) Wang, Y.; Wang, X.; Ghosh, S. K.; Lu, H. P. Probing Single-Molecule Interfacial Electron Transfer Dynamics of Porphyrin on TiO_2 Nanoparticles. *J. Am. Chem. Soc.* **2009**, *131*, 1479−1487.
(80) Guo, L.; Wang, Y.; Lu, H. P. Combined Single-Molecule Photon-Stamping Spectroscopy and Femtosecond Transient Absorption Spectroscopy Studies of Interfacial Electron Transfer Dynamics. *J. Am. Chem. Soc.* **2010**, *132*, 1999−2004.
(81) Paula, L. C.; Wang, J.; Leite, V. B. P. Statistics and Kinetics of Single-Molecule Electron Transfer Dynamics in Complex Environments: A Simulation Model Study. *J. Chem. Phys.* **2008**, *129*, 224504-1−224504-9.
(82) Leite, V. B. P.; Alonso, L. C. P.; Newton, M.; Wang, J. Single Molecule Electron Transfer Dynamics in Complex Environments. *Phys. Rev. Lett.* **2005**, *95*, 118301-1−118301-4.
(83) Kalyanasundaram, K.; Vlachopoulos, N.; Krishnan, V.; Monnier, A.; Grätzel, M. Sensitization of TiO_2, in the Visible Light Region Using Zinc Porphyrins. *J. Phys. Chem.* **1987**, *91*, 2342−2347.
(84) Savenije, T. J.; Goossens, A. Hole Transport in Porphyrin Thin Films. *Phys. Rev. B* **2001**, *64*, 115323-1−115323-9.
(85) Rochford, J.; Galoppini, E. Zinc(II) Tetraarylporphyrins Anchored to TiO_2, ZnO, and ZrO_2Nanoparticle Films through Rigid-Rod Linkers. *Langmuir* **2008**, *24*, 5366−5374.
(86) Rangan, S.; Coh, S.; Bartynski, R. A.; Chitre, K. P.; Galoppini, E.; Jaye, C.; Fischer, D. Energy Alignment, Molecular Packing, and Electronic Pathways: Zinc(II) Tetraphenylporphyrin Derivatives Adsorbed on TiO_2(110) and ZnO(11−20) Surfaces. *J. Phys. Chem. C* **2012**, *116*, 23921−23930.
(87) Li, L.-L.; Diau, E. W.-G. Porphyrin-Sensitized Solar Cells. *Chem. Soc. Rev.* **2013**, *42*, 291−304.
(88) Campbell, W. M.; Burrell, A. K.; Officer, D. L.; Jolley, K. W. Porphyrins as Light Harvesters in the Dye-Sensitised TiO_2 Solar Cell. *Coord. Chem. Rev.* **2004**, *248*, 1363−1379.
(89) Duonghong, D.; Borgarello, E.; Grätzel, M. Dynamics of Light-Induced Water Cleavage in Colloidal Systems. *J. Am. Chem. Soc.* **1981**, *103*, 4685−4690.
(90) Lu, H. P. Sizing Up Single-Molecule Enzymatic Conformational Dynamics. *Chem. Soc. Rev.* **2014**, *43*, 1118−1143.
(91) Pan, D.; Hu, D.; Lu, H. P. Probing Inhomogeneous Vibrational Reorganization Energy Barriers of Interfacial Electron Transfer. *J. Phys. Chem. B* **2005**, *109*, 16390−16395.
(92) Pan, D.; Klymyshyn, N.; Hu, D.; Lu, H. P. Tip-Enhanced Near-Field Raman Spectroscopy Probing Single Dye-Sensitized TiO_2 Nanoparticles. *Appl. Phys. Lett.* **2006**, *88*, No. 093121.
(93) Sevinc, P. C.; Wang, X.; Wang, Y.; Zhang, D.; Meixner, A. J.; Lu, H. P. Simultaneous Spectroscopic and Topographic Near-Field Imaging of TiO_2 Single Surface States and Interfacial Electronic Coupling. *Nano Lett.* **2011**, *11*, 1490−1494.
(94) Wang, J.; Wolynes, P. G. Intermittency of Single Molecule Reaction Dynamics in Fluctuating Environments. *Phys. Rev. Lett.* **1995**, *74*, 4317−4320.
(95) Leite, V. B. P.; Onuchic, J. N.; Stell, G.; Wang, J. Probing the Kinetics of Single Molecule Protein Folding. *Biophys. J.* **2004**, *87*, 3633−3641.
(96) Wang, J.; Xu, L.; Xue, K.; Wang, E. Exploring the Origin of Power Law Distribution in Single-Molecule Conformation Dynamics: Energy Landscape Perspectives. *Chem. Phys. Lett.* **2008**, *463*, 405−409.
(97) Wang, J.; Wolynes, P. G. Intermittency of Activated Events in Single Molecules: The Reaction Diffusion Description. *J. Chem. Phys.* **1999**, *110*, 4812−4819.
(98) Anderson, N. A.; Ai, X.; Chen, D. T.; Mohler, D. L.; Lian, T. Bridge-Assisted Ultrafast Interfacial Electron Transfer to Nanocrystalline SnO_2 Thin Films. *J. Phys. Chem. B* **2003**, *107*, 14231−14239.
(99) Asbury, J. B.; Hao, E.; Wang, Y.; Lian, T. Bridge Length-Dependent Ultrafast Electron Transfer from Re Polypyridyl Complexes to Nanocrystalline TiO_2 Thin Films Studied by Femtosecond Infrared Spectroscopy. *J. Phys. Chem. B* **2000**, *104*, 11957−11964.
(100) Moser, J. E. Dynamics of Interfacial and Surface Electron Transfer Processes. In *Dye-Sensitized Solar Cells*; Kalyanasundaram, K., Ed.; EPFL Press: Lausanne, Switzerland, 2010; pp 403−456 and references therein.
(101) Piotrowiak, P.; Galoppini, E.; Wei, Q.; Meyer, G. J.; Wiewiór, P. Subpicosecond Photoinduced Charge Injection from "Molecular Tripods" into Mesoporous TiO_2 Over the Distance of 24 Angstroms. *J. Am. Chem. Soc.* **2003**, *125*, 5278−5279.
(102) Lu, H. P.; Xie, X. S. Single-Molecule Kinetics of Interfacial Electron Transfer. *J. Phys. Chem. B* **1997**, *101*, 2753−2757.
(103) Issac, A.; Jin, S. Y.; Lian, T. Q. Intermittent Electron Transfer Activity From Single CdSe/ZnS Quantum Dots. *J. Am. Chem. Soc.* **2008**, *130*, 11280−11281.

(104) Cui, S. C.; Tachikawa, T.; Fujitsuka, M.; Majima, T. Interfacial Electron Transfer Dynamics in a Single CdTe Quantum Dot-Pyromellitimide Conjugate. *J. Phys. Chem. C* **2008**, *112*, 19625−19634.
(105) Xu, W.; Kong, J. S.; Yeh, Y.-T. E.; Chen, P. Single-Molecule Nanocatalysis Reveals Heterogeneous Reaction Pathways and Catalytic Dynamics. *Nat. Mater.* **2008**, *7*, 992−996.
(106) Kuno, M.; Fromm, D. P.; Hamann, H. F.; Gallagher, A.; Nesbitt, D. J. "On"/"Off" Fluorescence Intermittency of Single Semiconductor Quantum Dots. *J. Chem. Phys.* **2001**, *115*, 1028−1040.
(107) Hoogenboom, J. P.; Hernando, J.; van Dijk, E. M. H. P.; van Hulst, N. F.; García-Parajó, M. F. Power-Law Blinking in the Fluorescence of Single Organic Molecules. *ChemPhysChem* **2007**, *8*, 823−833.
(108) Margolin, G.; Barkai, E. Single-Molecule Chemical Reactions: Reexamination of the Kramers Approach. *Phys. Rev. E* **2005**, *72*, No. 025101 (R).
(109) Margolin, G.; Barkai, E. Aging Correlation Functions for Blinking Nanocrystals, and other On−Off Stochastic Processes. *J. Chem. Phys.* **2004**, *121*, 1566−1577.
(110) Tang, J.; Marcus, R. A. Diffusion-Controlled Electron Transfer Processes and Power-Law Statistics of Fluorescence Intermittency of Nanoparticles. *Phys. Rev. Lett.* **2005**, *95*, 107401−107404.
(111) Tang, J.; Marcus, R. A. Mechanisms of Fluorescence Blinking in Semiconductor Nanocrystal Quantum Dots. *J. Chem. Phys.* **2005**, *123*, 054704-1−054704-12.
(112) Luong, A. K.; Gradinaru, C. C.; Chandler, D. W.; Hayden, C. C. Simultaneous Time-and Wavelength-Resolved Fluorescence Microscopy of Single Molecules. *J. Phys. Chem. B* **2005**, *109*, 15691−15698.
(113) Novotny, L. Single Molecule Fluorescence in Inhomogeneous Environments. *Appl. Phys. Lett.* **1996**, *69*, 3806−3808.
(114) Liu, F.; Meyer, G. J. A Nuclear Isotope Effect for Interfacial Electron Transfer: Excited-State Electron Injection from Ru Ammine Compounds to Nanocrystalline TiO_2. *J. Am. Chem. Soc.* **2005**, *127*, 824−825.
(115) Watson, D. F.; Marton, A.; Stux, A. M.; Meyer, G. J. Influence of Surface Protonation on the Sensitization Efficiency of Porphyrin-Derivatized TiO_2. *J. Phys. Chem. B* **2004**, *108*, 11680−11688.
(116) Chizhik, A. I.; Gregor, I.; Schleifenbaum, F.; Muller, C. B.; Roling, C.; Meixner, A. J.; Enderlein, J. Electrodynamic Coupling of Electric Dipole Emitters to a Fluctuating Mode Density within a Nanocavity. *Phys. Rev. Lett.* **2012**, *108*, 163002-1−163002-4.
(117) Zhang, D.; Heinemeyer, U.; Stanciu, C.; Sackrow, M.; Braun, K.; Hennemann, L. E.; Wang, X.; Scholz, R.; Schreiber, F.; Meixner, A. J. Nanoscale Spectroscopic Imaging of Organic Semiconductor Films by Plasmon-Polariton Coupling. *Phys. Rev. Lett.* **2010**, *104*, 056601-1−056601-4.
(118) Grätzel, M.; Moser, J. E. In *Electron Transfer in Chemistry*; Balzani, V., Gould, I. R., Eds.; Wiley-VCH: Weinheim, Germany, 2001; Vol. 5, pp 589−644.
(119) Singh, R. S.; Tachiya, M.; Bagchi, B. Polarization Caging in Diffusion-Controlled Electron Transfer Reactions in Solution. *J. Phys. Chem. B* **2010**, *114*, 12284−12292.
(120) Denny, R. A.; Bagchi, B.; Barbara, P. F. Effects of Vibrational Energy Relaxation and Reverse Reaction on Electron Transfer Kinetics and Fluorescence Line Shapes in Solution. *J. Chem. Phys.* **2001**, *115*, 6058−6071.
(121) Bagchi, B.; Gayathri, N. Interplay between Ultrafast Polar Solvation and Vibrational Dynamics in Electron Transfer Reactions: Role of High-Frequency Vibrational Modes. *Adv. Chem. Phys.* **1999**, *107*, 1−80.
(122) Nandi, N.; Bhattacharyya, K.; Bagchi, B. Dielectric Relaxation and Solvation Dynamics of Water in Complex Chemical and Biological Systems. *Chem. Rev.* **2000**, *100*, 2013−2046.